Turkish Journal of Electrical Engineering & Computer Sciences

http://journals.tubitak.gov.tr/elektrik/

Research Article

Turk J Elec Eng & Comp Sci
(2021) 29: 257 – 275

doi:10.3906/elk-2004-145

Robust model reference adaptive PI controller based sliding mode control for three-phase grid connected photovoltaic inverter

Mojtaba MOETI, Mehdi ASADI*
Electrical Engineering Department, Engineering Faculty, Arak University of Technology, Arak, Iran

Received: 22.04.2020 • **Accepted/Published Online:** 04.08.2020 • **Final Version:** 27.01.2021

Abstract: In this paper, the design of a new robust model reference adaptive PI (MRAC-PI) current controller is proposed for a two-stage grid connected photovoltaic (PV) inverter. Perturb & observe (P&O) algorithm is implemented in the boost part in order to extract the maximum power from the PV array. Firstly, the current dynamics with considering the system uncertainties are written in dq frame and are simplified by employing a decoupling system. Then, the MRAC-PI controller is designed based on a sliding mode control (SMC) to improve the robustness of the controller under system uncertainties. The parameters of PI controller are tuned based on SMC laws to track the desired reference model and provides fast and desirable dynamic response. The stability of the robust MRAC-PI is proven by using Lyapunov's theory and Barbalet's lemma. Finally, the performance of the proposed current controller and the conventional PI based voltage oriented control (VOC) during variations in filter inductance and solar irradiance are compared through simulation results. These results show the effectiveness of the proposed controller.

Key words: Grid connected photovoltaic inverter, robust model reference adaptive PI controller, sliding mode control, decoupling system, Lyapunov's theory

1. Introduction

Because of the limitations on the use of fossil fuels, there has been an increase on the application of grid connected PV systems [1]. In spite of the advantages of PV arrays, it is a major issue to extract the maximum power from PV arrays. Also the integration of PV arrays that are dependent on the weather conditions can affect the stability, power quality, and reliability of the power grid. Therefore, it is necessary to design a proper robust and efficient current controller and maximum power point tracker (MPPT) algorithms [2]. A broad range of literature proposes various MPPT techniques and current controllers to control grid connected PV systems [3–5].

The PI controller is an effective and simple current controller and widely used in industries. However, the exact linearizing the system, the integrity of current decoupling, the precise tuning of PI coefficients, and lack of robustness are limited PI controller based approach [6]. Hence, recent researches in the direction of current controllers design have been focused on the robust and adaptive control methods.

In [7], a new control method is used in two stage grid connected PV system. In this method, the input disturbances caused in the dc link voltage are rejected by employing an adaptive P&O algorithm and the grid distortions and parametric uncertainty are handled by an integral sliding mode current controller. Although an integral sliding surface minimizes the steady state errors, the chattering problem could also exist. To enhance the

*Correspondence: mehdiasadi.email@gmail.com

GC-VSI robustness and reduce chattering problem, an improved current SMC controller with the exponential reaching law-based saturation function is proposed in [8]. However, the exact design of boundary layer is limited in this suggestion. In [9], a modified SMC current controller is proposed for shunt active power filters (SAPF). In order to improve SAPF robustness, an exponential reaching law is employed and to reduce the chattering phenomenon, a repetitive control (RC) term of harmonic current error is introduced to the sliding mode surface. Although the proposed surface can compensate all AC harmonic current, the design procedures of the proposed method are more complicated than classic SMC method. In [10], to have a robust current controller in three-phase grid connected PV system, the grid impedance variations is modelled as multiplicative disturbance, and then a H_∞ method is proposed. The complexity in the design of weighting functions is accounted as a main problem of this method. In [11], a robust deadbeat predictive current controller is proposed for a three-phase converter. To overcome the parameter uncertainties under unbalanced grid conditions, a discrete time power disturbance observer is designed. This method has shown a fast dynamics response and acceptable stability margin but has some disadvantages such as needs to know exact model of the system and a great number of calculations. To provide appropriate performances in the presence of disturbances in a voltage source converter, a simple MRAC current control is presented in [12]. This method has only one adaption gain and the stability of system is proved by Lyapunov theory. The tuning of controller gains through a trial and error approach is a hard and time consuming task. In order to eliminate the disadvantages of VOC method, a self tuning (ST) adaptive control is presented for a GC-VSI and is replaced with the PI controllers in the current loops of VOC method [13]. In the proposed method firstly, recursive least square (RLS) on line estimator is used to estimate the parameters of the system, and then control gains are updated based on the estimated values. Also, pole shift controller is employed to enhance system stability. The necessity of tuning at least five adaption gains and high online computational requirements are the major drawbacks of this controller. Recently, several robust hybrid methods have been developed for improving the robust performance of system in the presence of system uncertainties. In [14, 15], a new adaptive discrete SMC control is employed for uncertain nonlinear systems. To guarantee the stability of the system, a neuron online estimation of the errors in the sliding function is proposed. Also, the chattering phenomenon is reduced by adaptation of the switching gain.

To improve the robustness of discrete MRAC method based on RLS algorithm in a GC-VSI, a sliding mode action is added to the current controller [16]. This method guarantees the system stability in the presence of uncertainties. In [17], an improved MRAC-PR current controller for grid connected PV inverter with LCL filter is presented. In the proposed method, the PR parameters are regulated based on ant lion optimization (ALO) algorithm. With the help of proposed controller, damping resonance, proper transient performance, and enough stability margin are obtained. In [18], a novel adaptive PI current controller is employed in a microgrid to stabilize the magnitude and frequency of the voltage across the loads. Also, the parameters of PI controllers are adapted using least mean fourth (LMF) algorithm to improve system stability at different loading conditions. In [19], a combined MRAC and PI controller is proposed for a grid connected PV system with LCL filter. The system dynamic equations and the reference model are written in abc frame and the controller parameters are tuned by MIT rules.This controller guarantees the safe operation under different load conditions. To provide robust performance against parametric variations in a GC-VSI with LCL filter, an adaptive PI based particle swarm optimization (PSO) is presented in [20]. Despite the appropriate response of this method, its efficiency is dependent on the predefined parameters and necessitates expertise to obtain the desired response. In [21], an adaptive fuzzy PI controller is proposed for a grid connected PV inverter with irradiance variations. The parameters of PI controller are online tuned based on improved fuzzy logic.

Although the proposed method provides fast transient responses and strong stability are obtained independent from system parameters, implementation of this controller may become difficult if the training data is not available.

This paper introduces the innovation of MRAC-PI controller for a three-phase GC-VSI. The motivation for designing the proposed controller is to obtain desired performance against system disturbances such that simplicity in controller design and ease of tuning are provided. To obtain this goal, the concept of MRAC-PI controller based on SMC is introduced in this paper.

The key contribution of this paper is to provide an offline design procedure for proposed MRAC-PI controllers applied to GC-VSI under system uncertainties. In the beginning, by using the decoupling controllers, the effects of coupling terms are canceled, and the system model is written as a first order plant in the presence of matched uncertainties and positive constant terms. Then, a proportional sliding surface is selected and the PI coefficients are automatically tuned by the d axis current error and q axis current error. The upper bounds on the uncertainties are assumed to be known and the stability of the proposed controller is obtained using Lyapunov's theory and Barbalet's lemma. In comparison to the classical VOC, which is expressed in [13], the proposed controller provides better mitigation of harmonics, faster dynamic responses, and robustness to system uncertainties.

This paper is organized as follows: The model of the grid connected PV system and a decoupling system implementation with system uncertainties are presented in Section 2; in Section 3, a proposed robust MRAC-PI controller for GC-VSI is designed; Section 4 presents the simulation results on a 5 kW prototype GC-VSI to demonstrate the effectiveness of the proposed controller. Finally, the conclusions are drawn in Section 5.

2. Three phase GC-VSI modelling

Figure 1 shows a two-stage grid connected PV system where all power electronic elements are assumed to be ideal. The first stage is the boost converter, which increases the output voltage of the PV arrays and uses the MPPT control. The second stage is the inverter, which converts dc power into ac power and uses the proposed MRAC-PI current controller. The PV arrays used in this work are a type of Canadian solar CS6X-310P. Two parallel strings are used where each one includes 9 series modules. The PV array characteristic curves under various values of radiation levels and fixed value of temperature (25 °C) are shown in Figure 2. The GC-VSI dynamic model in abc frame can be expressed as (1).

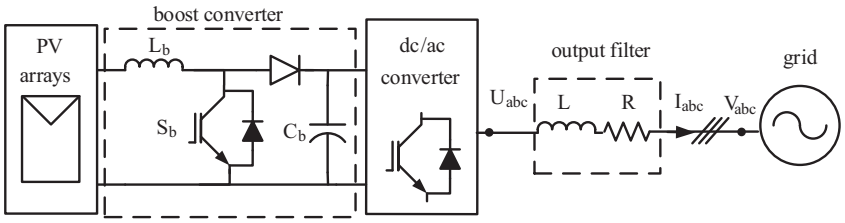

Figure 1. Three-phase grid connected PV system.

$$\begin{cases} \dfrac{dI_{abc}}{dt} = -\dfrac{R}{L}.I_{abc} + \dfrac{U_{abc}}{L} - \dfrac{V_{abc}}{L} \\ C_b\dfrac{dV_{dc}}{dt} = \dfrac{U_aI_a + U_bI_b + U_cI_c}{V_{dc}} \end{cases} \tag{1}$$

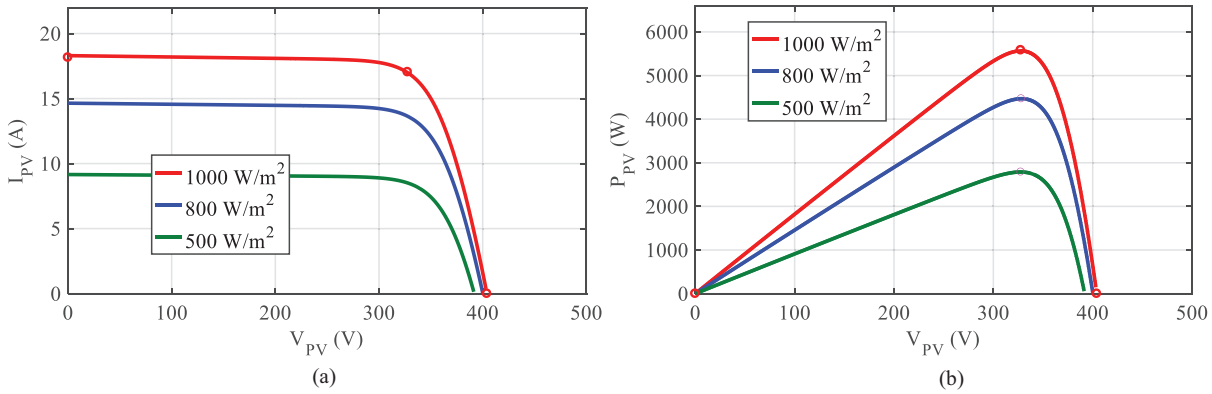

Figure 2. (a) Current-Voltage (I-V) curve (b) Power–Voltage (P-V) curve.

L, R are resistance and inductance of the filter, respectively; L_b, C_b, S_b are the inductance, capacitance, and switch of the boost converter, respectively; V_{abc} and U_{abc} are the grid and VSI terminals voltages, respectively; I_{abc} are the grid currents.

The current dynamics of the GC-VSI in dq frame using the Park's transformation $[T_{dq}]$ presented in (2), is expressed as (3).

$$[T_{dq}] = \frac{2}{3}\begin{bmatrix} \cos\omega t & \cos(\omega t - \frac{2\pi}{3}) & \cos(\omega t + \frac{2\pi}{3}) \\ \sin\omega t & \sin(\omega t - \frac{2\pi}{3}) & \sin(\omega t + \frac{2\pi}{3}) \\ \frac{1}{2} & \frac{1}{2} & \frac{1}{2} \end{bmatrix} \tag{2}$$

$$\begin{bmatrix} \dot{I}_d \\ \dot{I}_q \end{bmatrix} = \begin{bmatrix} -\frac{R}{L} & \omega \\ -\omega & -\frac{R}{L} \end{bmatrix} \begin{bmatrix} I_d \\ I_q \end{bmatrix} + \begin{bmatrix} \frac{1}{L} & 0 \\ 0 & \frac{1}{L} \end{bmatrix} \begin{bmatrix} u_d \\ u_q \end{bmatrix} \tag{3}$$

By defining $U_{dc} = \frac{C_b}{3V_d} V_{dc}^2$ and using (2), the dynamics of dc voltage in dq frame is given by (4).

$$\frac{dU_{dc}}{dt} = -\frac{2}{C_b} U_{dc} + I_d \tag{4}$$

Here, u_d and u_q are the outputs from the controllers of I_d and I_q, respectively. These new inputs are defined as $u_{dq} = [U_d - V_d \, U_q - V_q]^T$. $V_{dq} = [V_d \, V_q]^T$, $I_{dq} = [I_d \, I_q]^T$ and $U_{dq} = [U_d \, U_q]^T$ are grid voltages, grid currents, and inverter voltages in dq frame, respectively. ω is the angular frequency of the grid voltage. The Laplace transforms of (3) can be expressed as (5).

$$\begin{bmatrix} I_d(s) \\ I_q(s) \end{bmatrix} = \begin{bmatrix} G_{11}(s) & G_{12}(s) \\ G_{21}(s) & G_{22}(s) \end{bmatrix} \begin{bmatrix} u_d(s) \\ u_q(s) \end{bmatrix} \tag{5}$$

The transfer matrix G_{ij} is expressed as (6):

$$\begin{aligned} G_{11}(s) &= \frac{I_d}{u_d} = \frac{(Ls+R)}{L^2s^2+2RLs+(R^2+L^2\omega^2)} \\ G_{12}(s) &= \frac{I_d}{u_q} = \frac{L\omega}{L^2s^2+2RLs+(R^2+L^2\omega^2)} \\ G_{21}(s) &= \frac{I_q}{u_d} = \frac{-L\omega}{L^2s^2+2RLs+(R^2+L^2\omega^2)} \\ G_{22}(s) &= \frac{I_q}{u_q} = \frac{(Ls+R)}{L^2s^2+2RLs+(R^2+L^2\omega^2)} \end{aligned} \tag{6}$$

To eliminate $G_{12}(s)$ and $G_{21}(s)$, the decouplers $D_{12}(s)$ and $D_{21}(s)$ are proposed as (7).

$$\begin{cases} D_{12}(s) = -\dfrac{G_{12}(s)}{G_{11}(s)} = -\dfrac{L\omega}{Ls+R} \\ D_{21}(s) = -\dfrac{G_{21}(s)}{G_{22}(s)} = \dfrac{L\omega}{Ls+R} \end{cases} \tag{7}$$

The decouplers $D_{12}(s)$ and $D_{21}(s)$ are taken in series with $G_{ij}(s)$ to produce a diagonal matrix $G_{n,ij}(s)$ as in (8).

$$\begin{bmatrix} I_d(s) \\ I_q(s) \end{bmatrix} = \begin{bmatrix} G_{n,11}(s) & 0 \\ 0 & G_{n,22}(s) \end{bmatrix} \begin{bmatrix} u_d(s) \\ u_q(s) \end{bmatrix} \tag{8}$$

$G_{n,11}(s)$ and $G_{n,22}(s)$ are shown in (9):

$$\begin{cases} G_{n,11}(s) = \dfrac{I_d(s)}{u_d(s)} = G_{11}(s) + D_{21}(s)G_{12}(s) = \dfrac{1}{[Ls+R]} \\ G_{n,22}(s) = \dfrac{I_q(s)}{u_q(s)} = G_{22}(s) + D_{12}(s)G_{21}(s) = \dfrac{1}{[Ls+R]} \end{cases} \tag{9}$$

The continues time representation of a diagonal matrix (8) can be expressed as (10).

$$\begin{cases} \dot{I}_d = -a_d I_d + b_d u_d \\ \dot{I}_q = -a_q I_q + b_q u_q \end{cases} \tag{10}$$

$a_d = a_q = -R/L$ and $b_d = b_q = -1/L$. Because of existence of noise and inductance variations, the state space model of the GC-VSI in (10), can be written as (11).

$$\begin{cases} \dot{I}_d = -(a_d + \Delta a_d)I_d + (b_d + \Delta b_d)u_d + f_d \\ \dot{I}_q = -(a_q + \Delta a_q)I_q + (b_q + \Delta b_q)u_q + f_q \end{cases} \tag{11}$$

Where, Δa_d, Δb_d, Δa_q and Δb_q are uncertainties in a_d, b_d, a_q and b_q, respectively. f_d and f_q show external disturbances. Let z_{1d}, z_{2d}, z_{1q}, z_{2q} be $\dot{I}_d$, u_d, $\dot{I}_q$, u_q, respectively. Then, define another output vectors

$d_{1q} = \Delta a_q \dot{I}_d$, $d_{2d} = \Delta b_d u_d$, $d_{1q} = \Delta a_q \dot{I}_q$, and $d_{2q} = \Delta b_q u_q$. By these considerations, the disturbed modeling of (11) can be rewritten as (12).

$$\begin{bmatrix} z_{1d}(s) \\ z_{1q}(s) \end{bmatrix} = \begin{bmatrix} a_d & 0 \\ 0 & a_q \end{bmatrix} \begin{bmatrix} I_d(s) \\ I_q(s) \end{bmatrix} + \begin{bmatrix} 1 & 1 & 0 & 0 \\ 0 & 0 & 0 & 0 \\ 0 & 0 & 1 & 1 \\ 0 & 0 & 0 & 0 \end{bmatrix} \begin{bmatrix} d_{1d} \\ d_{2d} \\ d_{1q} \\ d_{2q} \end{bmatrix} + \begin{bmatrix} b_d & 0 \\ 0 & b_q \end{bmatrix} \begin{bmatrix} u_d \\ u_q \end{bmatrix} + \begin{bmatrix} f_d \\ f_q \end{bmatrix} \tag{12}$$

To design the proposed MRAC-PI controller, the matching condition is assumed to be satisfied in the uncertainties Δa_d, Δb_d, Δa_q and Δb_q. In other words, there exist unknown scalers $d(t)$, $g(t)$, $q(t)$ and $h(t)$ such that the equations $\Delta a_d = b_d * d(t)$, $\Delta a_q = b_q * q(t)$, $\Delta b_d = b_d * g(t)$, $\Delta b_q = b_q * h(t)$ are obtained. By these considerations, the equation (11) can be rewritten as (13).

$$\begin{cases} \dot{I}_d = -a_d I_d + b_d u_d + b_d f_{d,m} + f_d \\ \dot{I}_q = -a_q I_q + b_q u_q + b_q f_{q,m} + f_q \end{cases} \tag{13}$$

The variables $f_{d,m}$ and $f_{q,m}$ denote the matched uncertainties and are expressed as (14).

$$\begin{cases} f_{d,m} = b_d d(t) + b_d g(t) \\ f_{q,m} = b_q q(t) + b_q h(t) \end{cases} \tag{14}$$

The matched uncertainties and the external disturbances in (13) are assumed to be bounded by some known positive constants ($\alpha_{d,m}$, $\alpha_{q,m}$, α_d, α_q), as expressed in (15).

$$\begin{cases} |f_{d,m}| \leq \alpha_{d,m} \ , \ |f_{q,m}| \leq \alpha_{q,m} \\ |f_d| \leq \alpha_d \ , \ |f_q| \leq \alpha_q \end{cases} \tag{15}$$

The structures of the close loop control of the decoupled GC-VSI without system disturbances and with them are shown in Figure 3. $G_{c1}(s)$ and $G_{c2}(s)$, are the current controllers, $u_{1,d}(s)$ and $u_{1,q}(s)$ are the control signals, and ${I_d}^*$ and ${I_q}^*$ are the reference values of I_d and I_q, respectively.

3. Design of the proposed controller

This section discusses the design of the grid connected PV system control scheme, i.e. MPPT design, dc link voltage control outer loop and proposed MRAC-PI current control loop. The control objectives of the proposed controller in the presence of system uncertainties are:

(1) To provide the adjustable transient responses and proper steady state responses.
(2) To guarantee stability characteristics of the GC-VSI.

The first stage in the design of the proposed robust MRAC-PI is to define a reference model as (16), of which the relative degree is the same as (10).

$$\dot{I}_{j,m} = -a_{j,m} I_{j,m} + b_{j,m} {I_j}^* \tag{16}$$

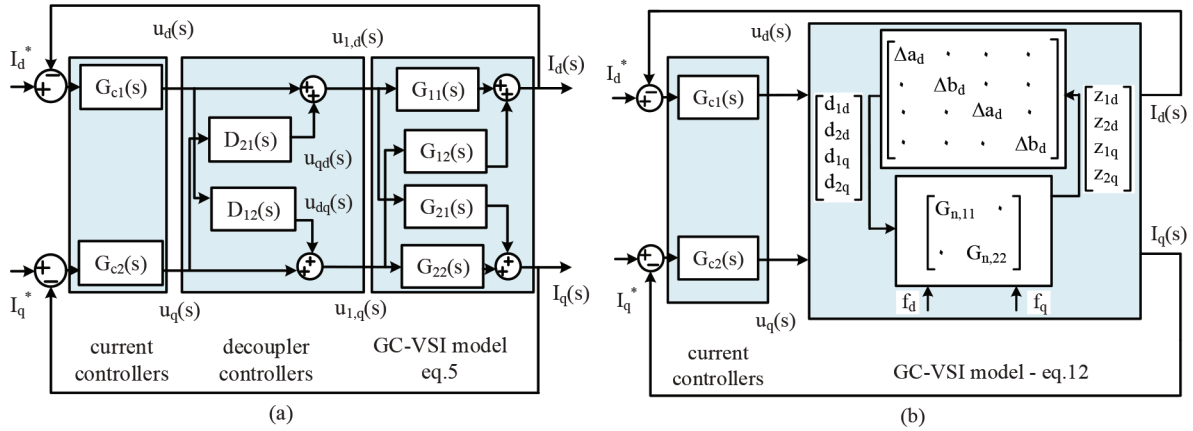

Figure 3. (a) Schematic of the GC-VSI control with decouplers (b) Structure of the close loop control of the decoupled GC-VSI with system disturbances.

, where $j = d, q$, ${I_j}^* \in R^1$ and $I_{j,m} \in R^1$ are the reference input and the output of the reference model, respectively. The variables $a_{j,m}$, $b_{j,m}$ are the scalers, which are determined based on desired dynamic responses.

Let the switching functions S_j be in the proportional forms as (17).

$$S_j = \lambda_j e_j = \lambda_j (I_j - I_{j,m}) \tag{17}$$

, where e_j and λ_j are the tracking error and the positive control gain in dq frame. The control objective here is to achieve an adaptive law so that S_j approaches to zero. By differentiating S_j, (18) is yielded.

$$\dot{S}_j = \lambda_j \dot{e}_j = -\lambda_j a_{j,m} e_j - \lambda_j (a_j - a_{j,m}) I_j - \lambda_j b_{j,m} {I_j}^* + \lambda_j b_j u_j + \lambda_j b_j f_{j,m} + \lambda_j f_j \tag{18}$$

The time derivative of S_j can also be written as (19).

$$\dot{S}_j = -\rho_j \mathrm{sgn}(S_j) \tag{19}$$

, where ρ_j is positive constant. By equaling (18) and (19), the input controller is called as (20).

$$\begin{aligned} u_j = {} & (\lambda_j b_j)^{-1} \lambda_j a_{j,m} e_j + (\lambda_j b_j)^{-1} \lambda_j (a_j - a_{j,m}) I_j - f_{j,m} - (\lambda_j b_j)^{-1} \lambda_j f_j \\ & + (\lambda_j b_j)^{-1} \lambda_j b_{j,m} {I_j}^* - \rho_j (\lambda_j b_j)^{-1} \mathrm{sgn}(S_j) \end{aligned} \tag{20}$$

It is assumed that there exist positive constants ${K_{p,j}}^*$ and ${K_{I,j}}^*$ such that the following matching conditions (21) between the plant (10) and the reference model (16) are satisfied.

$$\begin{cases} (-a_j - b_j {K_{p,j}}^* - b_j \dfrac{{K_{I,j}}^*}{s}) = -a_{j,m} \\ \\ (b_j {K_{p,j}}^* + b_j \dfrac{{K_{I,j}}^*}{s}) = b_{j,m} \end{cases} \tag{21}$$

From (21), the input controller (20) can be written as (22).

$$\begin{aligned} u_j = {} & (\lambda_j b_j)^{-1} \lambda_j a_{j,m} e_j + K^*_{P,j} [{I_j}^* - I_j] - f_{j,m} + K^*_{I,j} \int ({I_j}^* - I_j) - (\lambda_j b_j)^{-1} \lambda_j f_j \\ & - \rho_j (\lambda_j b_j)^{-1} \mathrm{sgn}(S_j) \end{aligned} \tag{22}$$

In the actual condition, ${K_{p,j}}^*$ and ${K_{I,j}}^*$ are not exactly known and are estimated by $K_{P,j}$ and $K_{I,j}$, respectively. Therefore, the input controller (22) is rewritten as (23).

$$\begin{aligned} u_j = {} & (\lambda_j b_j)^{-1}\lambda_j a_{j,m} e_j + K_{P,j}[{I_j}^* - I_j] - f_{j,m} + K_{I,j}\int ({I_j}^* - I_j) - (\lambda_j b_j)^{-1}\lambda_j f_j \\ & -\rho_j(\lambda_j b_j)^{-1}\mathrm{sgn}(S_j) \end{aligned} \tag{23}$$

In order to eliminate the effects of $f_{j,m}$ and f_j in input controller (23), the inequality (24) must be satisfied. Eventually the input controller is obtained as (25).

$$|\rho_j| \geq |\lambda_j|\,|\alpha_j| + (|\lambda_j b_j|)\,|\alpha_{j,m}| + \eta \tag{24}$$

$$u_j = (\lambda_j b_j)^{-1}\lambda_j a_{j,m} e_j + K_{P,j}[{I_j}^* - I_j] + K_{I,j}\int ({I_j}^* - I_j) - \rho_j(\lambda_j b_j)^{-1}\mathrm{sgn}(S_j) \tag{25}$$

The next phase of the proposed controller design is to estimate $K_{P,j}$ and $K_{I,j}$ by proper adaptive laws. First define the parameters error as (26). By substituting (26) into (25), u_j is rewritten as (27).

$$\begin{cases} \tilde{K}_{P,j}(t) = K_{P,j}(t) - K^*_{P,j} \\ \tilde{K}_{I,j}(t) = K_{I,j}(t) - K^*_{I,j} \end{cases} \tag{26}$$

$$\begin{aligned} u_j = {} & (\lambda_j b_j)^{-1}\lambda_j a_{j,m} e_j + [{K_{P,j}}^* + \tilde{K}_{P,j}][{I_j}^* - I_j] + [{K_{I,j}}^* + \tilde{K}_{I,j}]\int ({I_j}^* - I_j) \\ & -\rho_j(\lambda_j b_j)^{-1}\mathrm{sgn}(S_j) \end{aligned} \tag{27}$$

From (21) and by substituting (27) into (18), the time derivative S_j is rewritten as (28).

$$\begin{aligned} \dot{S}_j = \lambda_j \dot{e}_j = {} & \lambda_j b_j \tilde{K}_{P,j}(t)[{I_j}^* - I_j] + \lambda_j b_j \tilde{K}_{I,j}(t)\textstyle\int ({I_j}^* - I_j) - \rho_j \mathrm{sgn}(S_j) \\ & +\lambda_j b_j f_{j,m} + \lambda_j f_j \end{aligned} \tag{28}$$

Define a quadratic positive definite Lyapunov function as (29).

$$W_j = \frac{1}{2}S_j^2 + |\lambda_j b_j|\,[\gamma_{1,j}^{-1}\tilde{K}^2_{P,j}(t) + \gamma_{2,j}^{-1}\tilde{K}^2_{I,j}(t)] \tag{29}$$

, where $\gamma_{1,j}$ and $\gamma_{2,j}$ are positive scalers. The time derivative of $W_j(t)$ is obtained as shown in (30).

$$\begin{aligned} \dot{W} = {} & S_j\dot{S}_j + |\lambda_j b_j|\,\gamma_{1,j}^{-1}\tilde{K}_{P,j}(t)\dot{\tilde{K}}_{P,j}(t) + |\lambda_j b_j|\,\gamma_{2,j}^{-1}\tilde{K}_{I,j}(t)\dot{\tilde{K}}_{I,j}(t) \\ = {} & S_j\lambda_j b_j \tilde{K}_{P,j}(t)[{I_j}^* - I_j] + S_j\lambda_j b_j \tilde{K}_{I,j}(t)\int ({I_j}^* - I_j) \\ & -S_j\rho_j\mathrm{sgn}(S_j) + S_j\lambda_j b_j f_{j,m} + S_j\lambda_j f_j \\ & + |\lambda_j b_j|\,\gamma_{1,j}^{-1}\tilde{K}_{P,j}(t)\dot{\tilde{K}}_{P,j}(t) + |\lambda_j b_j|\,\gamma_{2,j}^{-1}\tilde{K}_{I,j}(t)\dot{\tilde{K}}_{I,j}(t) \end{aligned} \tag{30}$$

To ensure that the time derivative of $W_j(t)$ is always negative, the adaptive laws (31) are considered.

$$\begin{cases} \dot{K}_{P,j}(t) = -\gamma_{1,j}\text{sgn}(\lambda_j b_j) S_j [{I_j}^* - I_j] \\ \dot{K}_{I,j}(t) = -\gamma_{2,j}\text{sgn}(\lambda_j b_j) S_j [\int ({I_j}^* - I_j)] \end{cases} \tag{31}$$

By substituting (31) into (30), the time derivative of $W_j(t)$ can be written as (32).

$$\dot{W}_j = -S_j \rho_j \text{sgn}(S_j) + S_j \lambda_j b_j f_{j,m} + S_j \lambda_j f_j \tag{32}$$

The inequality of (33) holds in (32).

$$\begin{aligned} \dot{W}_j &\leq -\rho_j S_j \text{sgn}(S_j) + |S_j|\,|\lambda_j b_j|\,|f_{j,m}| + |S_j|\,|\lambda_j|\,|f_j| \\ &\leq -\rho_j\,|S_j| + |S_j|\,|\lambda_j b_j|\,|\alpha_{j,m}| + |S_j|\,|\lambda_j|\,|\alpha_j| \\ &\leq -|S_j|\,[\rho_j - |\lambda_j b_j|\,|\alpha_{j,m}| - |S_j|\,|\lambda_j|\,|\alpha_j|] \end{aligned} \tag{33}$$

From (24), the inequality of (33) is rewritten as (34).

$$\dot{W}_j \leq -\eta\,|S_j| \tag{34}$$

The equation (34) shows that the time derivative of $W_j(t)$ is always negative. According to Barbalat's Lemma, S_j approaches to zero in finite time. Consequently, the tracking error ($e_j(t) = I_{j,m} - I_j$) will converge to zero. To summarize the design procedure of the proposed MRAC-PI current controller, the flow diagram of the current controller is shown in Figure 4.

The schematic diagram of the system control scheme is illustrated in Figure 5. In the outer loop, a PI controller which produces ${I_d}^*$ is addressed to control the dc link voltage. To extract the maximum power from PV arrays under different environmental conditions, a P&O algorithm which was published in [1], is used.

4. Simulation results

To determine the effectiveness of the proposed MRAC-PI strategy which is modeled in Figure 6, simulation studies on a 5 kW prototype grid connected PV system are carried out in MATLAB/Simulink (MathWorks, Inc., Natick, MA, USA). The obtained results are compared with the classical VOC method that expressed in [13] under the following conditions: irradiance level variations, uncertainty in filter inductor. The parameters of the system are given in Table 1 and the parameters of the proposed controller, the conventional PI based VOC, and V_{dc} regulator are given in Table 2. With regard to the closed loop transfer functions of I_d and I_q dynamics, the parameters of PI controllers are designed such that the settling time $T_{s,j} = 9$ ms, $j = d, q$ and the damping ratios $\zeta_j = 1$, $j = d, q$ are provided. The model reference parameters in (16), the adaption gains, and the SMC parameters are designed based on the providing settling time $T_{s,j} = 3.5$ ms, a trial and error approach, and achieving the robust condition is shown in (24), respectively. Finally, a comparison of different control methods are given.

4.1. With sudden change in irradiance level

Figure 7 compares the system response during various irradiance level steps for the PI based VOC and proposed MRAC-PI controller. As shown in Figure 7, the irradiance level is stepped from $800 W/m^2$ to $1000 W/m^2$ at

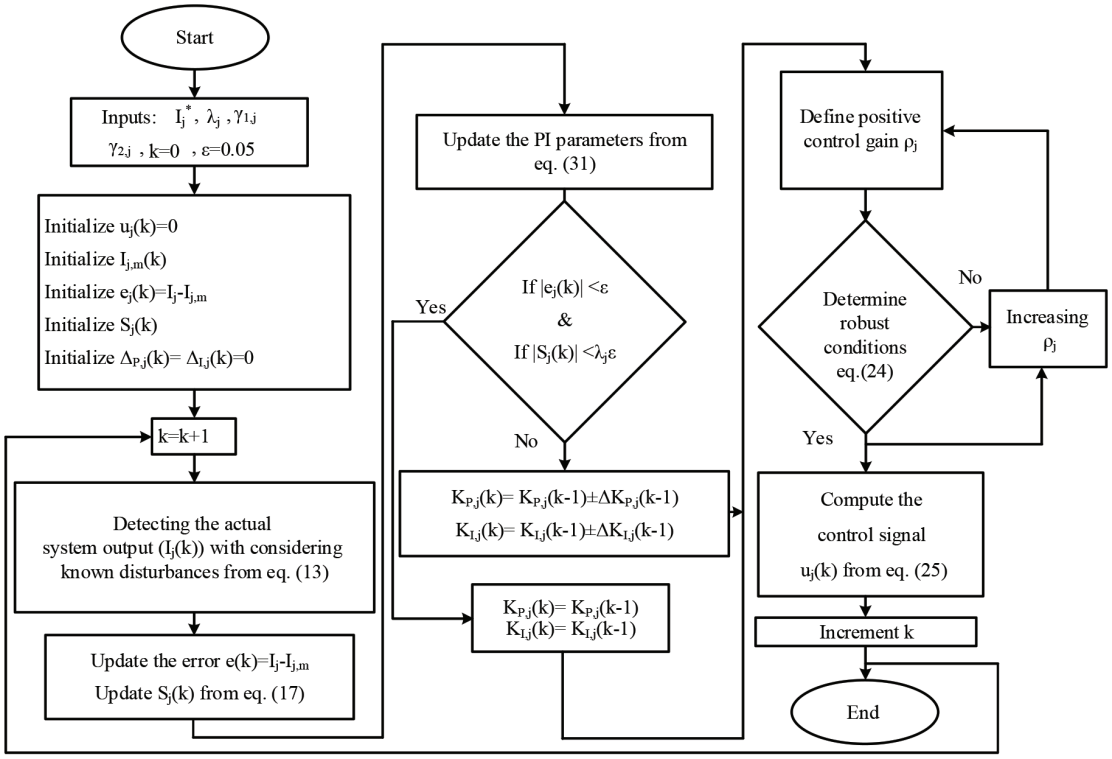

Figure 4. Flow diagram of the proposed controller strategy.

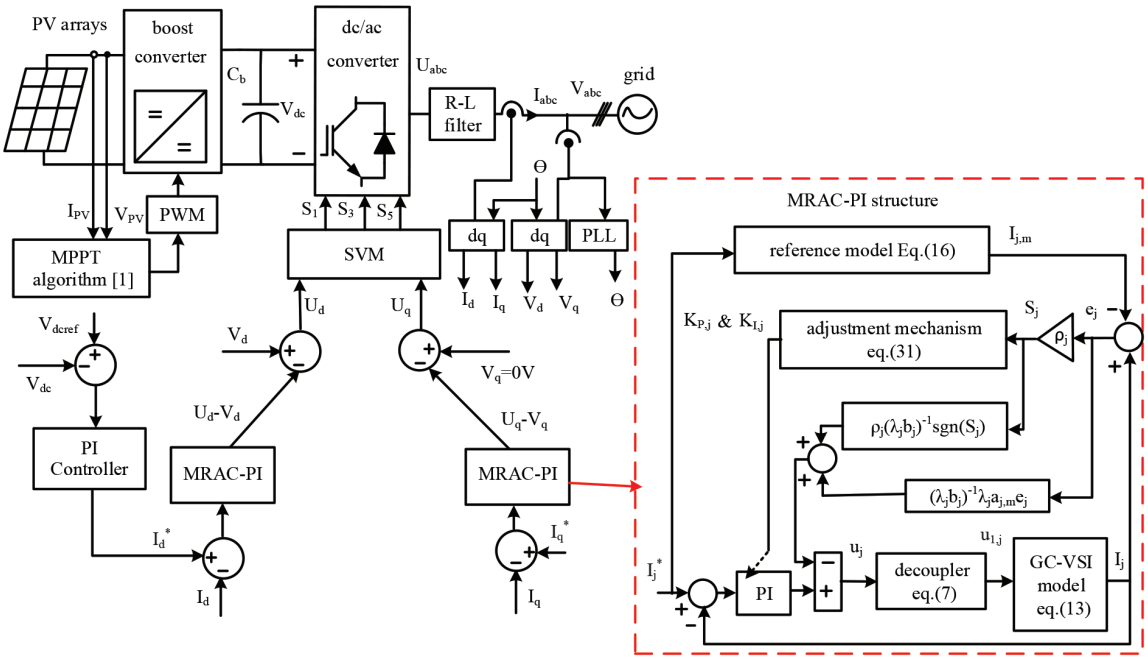

Figure 5. Control diagram of the grid connected PV system.

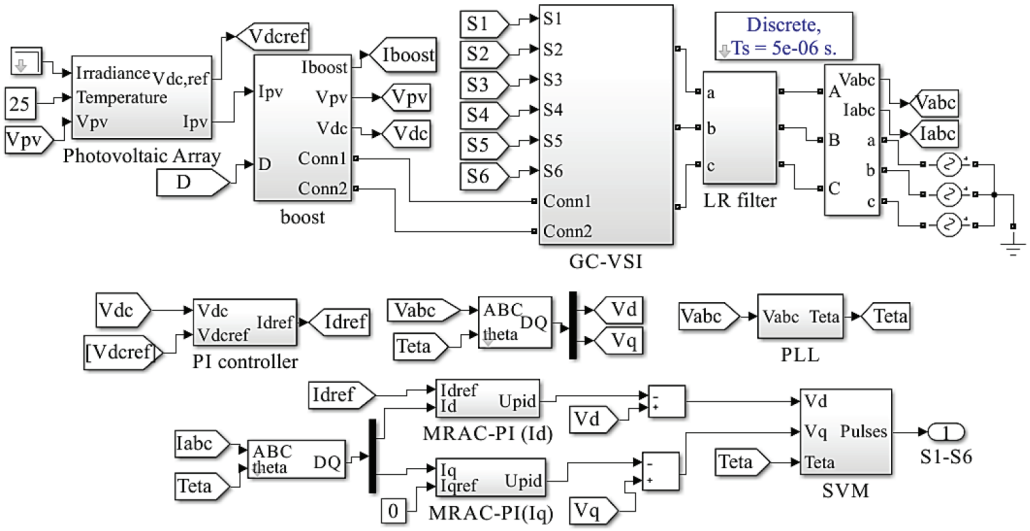

Figure 6. Simulink model of the proposed structure.

Table 1. Grid connected PV system parameters.

Parameter name	Symbol	Value
Rated power	S_n	5 kW
Grid voltage	V_{abc}	380 V
Grid frequency	f	50 Hz
Dc link voltage	V_{dc}	700 V
Dc link capacitor	C_b	2500 μF
inductor of boost converter	L_b	1 mH
Switching frequency of boost	f_{sw}	15 kHz
Filter resistance	R	0.05 Ω
Filter inductance	L	5 mH
Switching frequency of inverter	f_{sw}	15 kHz
Maximum power of PV module	P_{PV}	310.128 W
Voltage at maximum power point	V_{mp}	36.4 V
Current at maximum power point	I_{mp}	8.52 A
Open circuit voltage of PV module	V_{oc}	44.9 V
Short circuit current of PV module	I_{sc}	9.08 A

25 ms and then backed to $800W/m^2$ at 50 ms, while the q axis current reference is fixed at 0 A. As depicted in Figure 7, since the PI parameters in proposed controller are online tuned based on adaption SMC laws to converge errors to zero, less oscillation occur compared to conventional PI controller. In addition, the proposed controller provides faster transient responses than PI controller. Also, at the instant of the sudden change of irradiance no overshoot and undershoot are observed in proposed controller responses.

To be more specific from Figure 8, the PI controller in VOC method has overshoot and undershoot of 1 V and a settling time of 75 ms, while the proposed MRAC-PI method has a settling time of 35 ms as the

Table 2. Control parameters of the GC-VSI.

Controller	Parameter	Symbol	value
MRAC-PI Method	Model reference parameters	$a_{d,m}$, $b_{d,m}$	1500
		$a_{q,m}$, $b_{q,m}$	1500
	Adaption gains	$\gamma_{1,d}$	100
		$\gamma_{2,d}$	1500
		$\gamma_{1,q}$	150
		$\gamma_{2,q}$	500
	SMC parameters	λ_d, λ_q	0.3
		ρ_d	5000
		ρ_q	3000
VOC method	Proportional gains	$K_{P,d}$, $K_{P,q}$	878.888
	Integral gains	$K_{I,d}$, $K_{I,q}$	197530
V_{dc} regulator	Proportional gains	$K_{P,V_{dc}}$	0.1
	Integral gains	$K_{I,V_{dc}}$	20

reference model is defined and no overshoot and undershoot are observed.

According to the proof of proposed controller design in Section 3, the noninitialized coefficients of the PI current controller must converge fast to a constant value, and this is shown in Figure 9. In addition, at the instant of the sudden change of irradiance, the coefficients of d axis change slightly and then converge to a constant value.

To compare the performances of dc link voltage controller, the dc link voltage response of proposed controller and VOC method are shown in Figure 10. In spite of the proposed method, the dc link voltage changes a lot when irradiance levels are changed in VOC method.

4.2. With uncertainty in filter inductance

In this section, to investigate the proposed MRAC-PI controller robustness with regard to parameters changes, simulations are performed with filter inductance error equal to -25% in the interval between $t = 20$ and $t = 75$ ms. In this test, the solar radiation is fixed in $1000\,W/m^2$ and the q axis current reference is fixed in 0 A. The parameters of controllers are the same as the previous test.

Figure 11 shows the results of the two controllers with inductance variations. As seen in Figure 11, when the uncertainty occurs (20 ms to 75 ms), the grid current associated with the PI controller in VOC method has high distortion. Also, about 1.3 V undershoot in I_d is produced at 20 ms. These functions are duo to the dependence of PI controller coefficients on system conditions. But the proposed MRAC-PI controller automatically tunes the PI parameters and provides an improved grid current THD and no undershoot are produced in responses.

Variations of the coefficients of the proposed MRAC-PI controller with -25% error in inductance are depicted in Figure 12. These parameters are tuned online, so that I_d and I_q steady state errors bounded to desirable values when the uncertainty occurs. Furthermore, within the interval between $t = 20$ and $t = 75$ ms, the adaption mechanism rapidly reacts and increases to compensate I_d and I_q steady state errors and then the PI parameters converge to a positive constant.

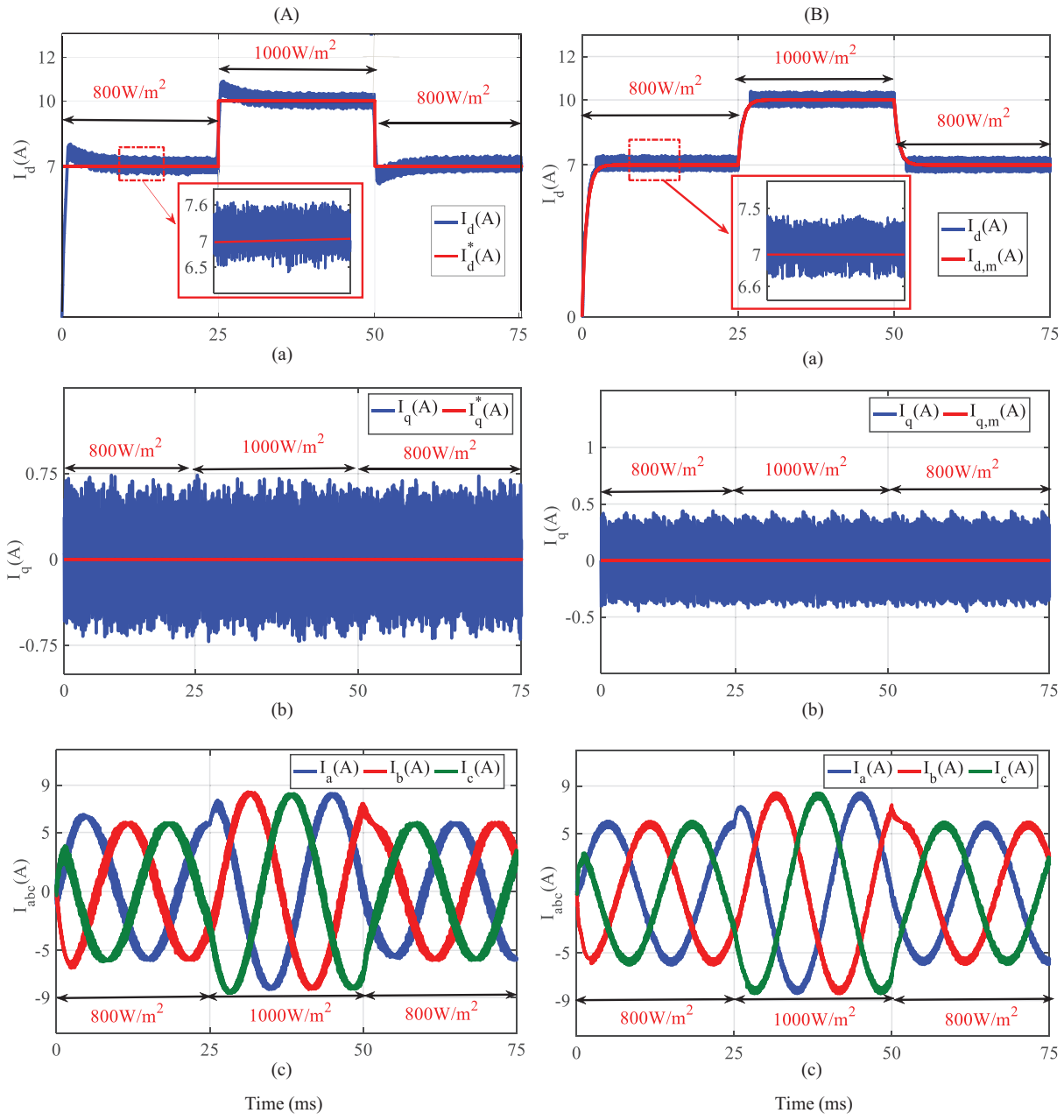

Figure 7. Simulation results using the two different control technics under $800 - 1000\,W/m^2$ solar radiation. (a) trajectories of I_d (A) (b) trajectories of I_q (A) (c) three phase ac currents (A). (A) PI controller in VOC method (B) Proposed controller.

To further compare the results of the two control strategies, Table 3 compares the grid current total harmonic distortion (THD) for the VOC method and proposed controller. As depicted in Table 3, the proposed controller provides lower grid current THD than VOC method.

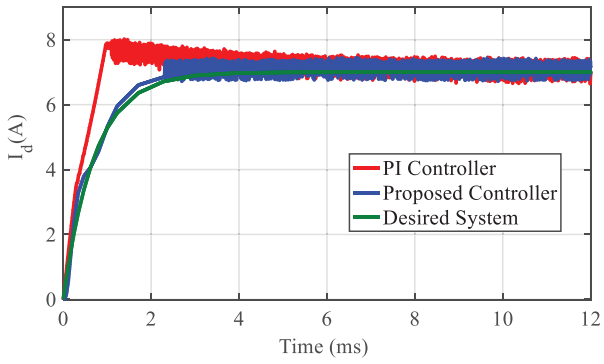

Figure 8. Evolution of the transient response of I_d for both VOC method and proposed controller.

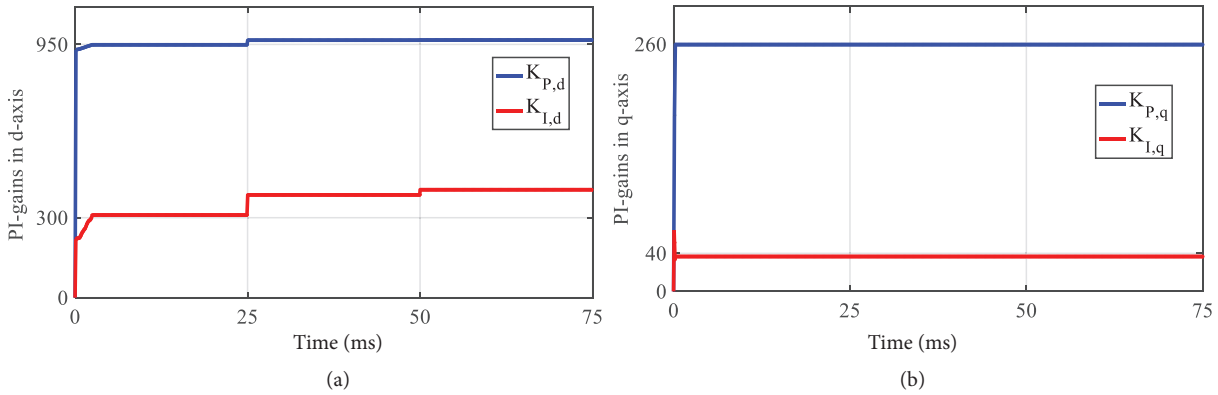

Figure 9. (a) d axis MRAC-PI controller (b) q axis MRAC-PI controller with sudden change in irradiance level.

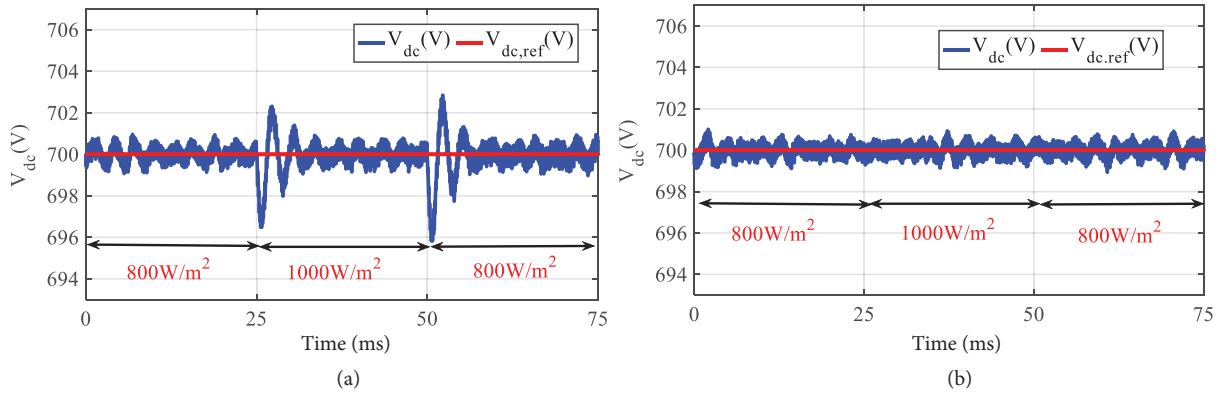

Figure 10. The waveforms of V_{dc} under using the two different control technics under $800-1000\,W/m^2$ solar radiation. (a) VOC method (b) proposed controller.

4.3. Comparison between proposed MRAC-PI current controller and robust hybrid controller

A comparison of the advantages and disadvantages between the robust hybrid controller which are given in Section 1 and the proposed method, is presented in Table 4. It is evident from Table 4 that the proposed controller has superior performance than other control methods. Also, the proposed robust MRAC-PI controller

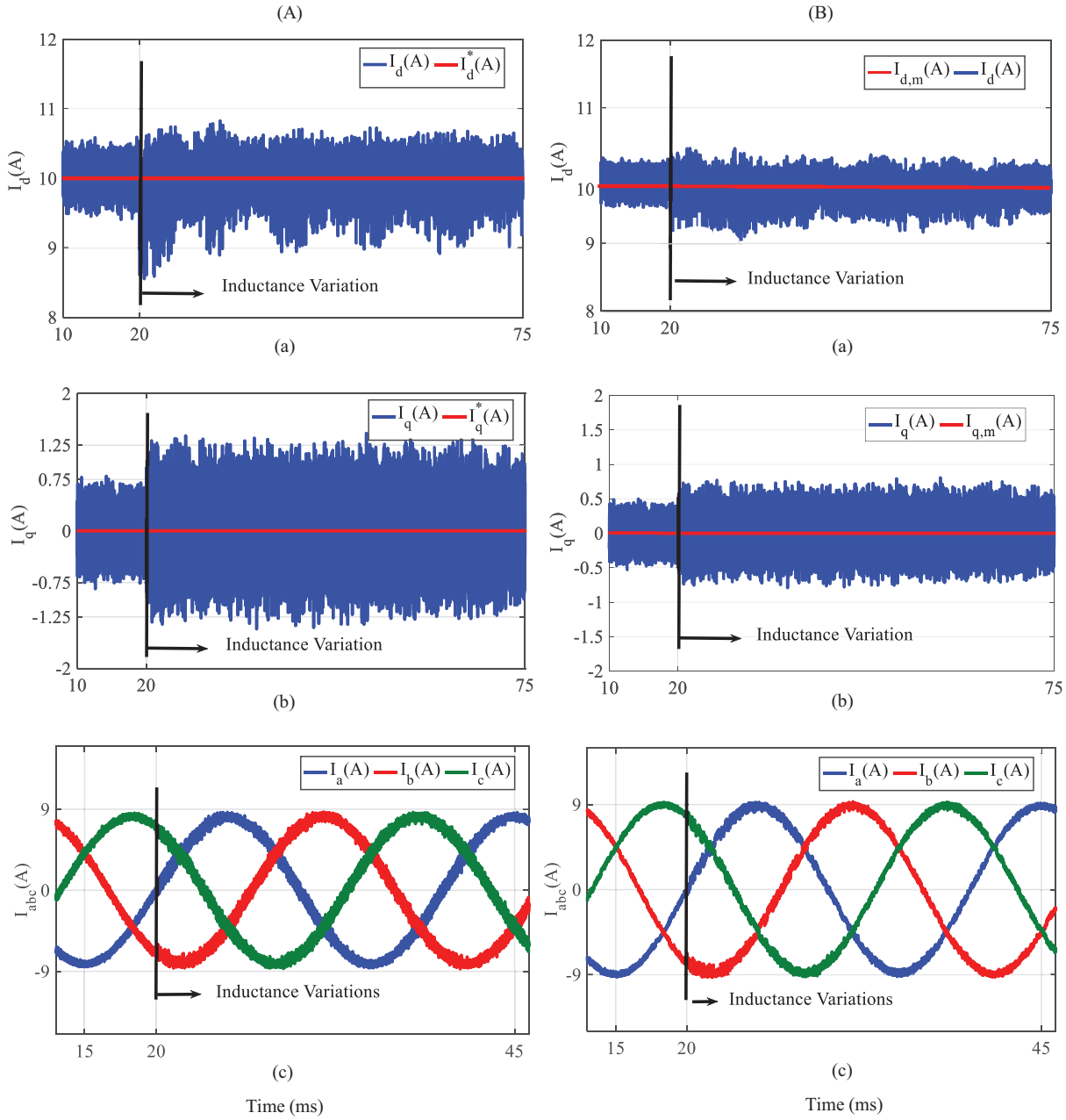

Figure 11. Simulation results using the two different control technics with -25% error in inductances. (a) trajectories of I_d (A) (b) trajectories of I_q (A) (c) three phase ac currents (A). (A) PI controller in VOC method (B) Proposed controller.

has less complexity than other control methods.

5. Conclusion

This paper presented a design procedure for robust decoupled MRAC-PI controllers applied to grid connected PV inverter under system uncertainties. In presented system, maximum power is transferred from PV arrays to

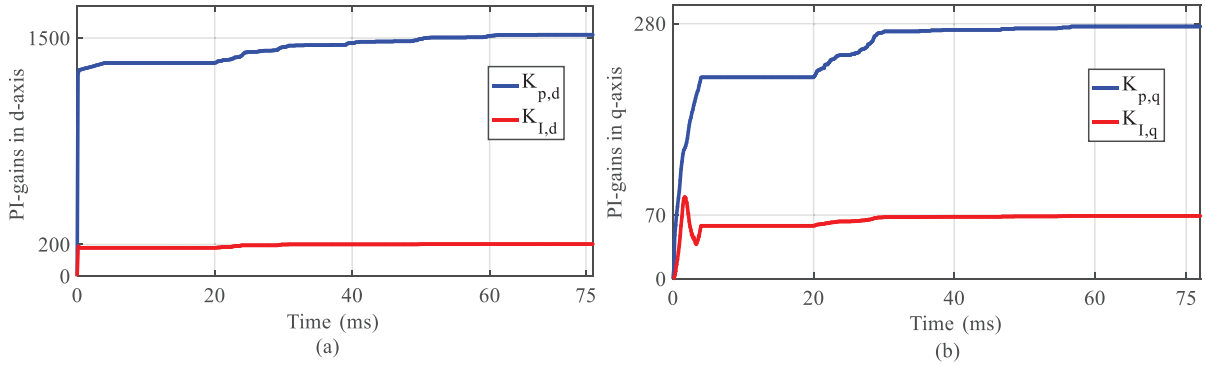

Figure 12. (a) d axis MRAC-PI controller (b) q axis MRAC-PI controller with -25% error in inductance.

Table 3. Grid current THD for the VOC method and robust MRAC-PI controllers under $\pm 25\%$ inductance variations.

Controller	% Inductance variations	Time interval	THD
Robust MRAC-PI	0	$0-20$ ms	2.8%
	-25%	$20-75$ ms	2.88%
	+25%	$20-75$ ms	1.5%
VOC method	0	$0-20$ ms	3.48%
	-25%	$20-75$ ms	4.98%
	+25%	$20-75$ ms	2.1%

the grid using P&O algorithm. The concept of SMC method is included in MRAC-PI controller to enhance the robustness of the controller. The proposed controller uses adaptive SMC laws to estimate the PI parameters online and offers a fast convergence of the sliding surface. The stability of this type of controller (robust hybrid controller) is proven by using Lyapunov's theory and Barbalet's lemma. The system responses of the proposed controller are compared with the PI controller in VOC method using MATLAB simulations in the presence of system uncertainties such as different levels of solar irradiance and filter inductance variations. From the simulation results, it is observed that fast convergence of PI parameters, desirable dynamic performance, and suitable steady state response are achieved without considering initial values for controller parameters. The proposed method also exhibits superior performance when compared with the PI controller in VOC strategy. The proposed controller is able to reduce the overshoot of I_d from 14.15% to 0% in simulation (under irradiance levels variations and fixed filter inductances). Further, the MRAC-PI controller is efficient to reduce the THD of grid current from 4.98% to 2.88% in simulation (under filter inductance variations and fixed irradiance levels). A comparison study of the advantages and disadvantages between the robust hybrid controller, which are recently presented, and the proposed method has proved that the proposed MRAC-PI controller provides robust performance and reduces the system complexities.

Table 4. Comparison of robust hybrid controller.

Reference	Control method	Advantage	Inconvenient
[14, 15]	Adaptive SMC	-Improve the robustness of classical SMC -Reduce the chattering phenomenon of classical SMC	-Complexity in design -Require high number of calculations
[16]	MRAC- SMC controller	-Improve the robustness of MRAC -Appropriated stability margin -Fast convergence of the controller parameters -Reduction in number of measurement sensors	-Requires accurate model of system -Complexity in design -Hard tuning of some adaption gains
[17]	MRAC- PR controller	-Damping resonance -Proper transient performance -Enough stability margin	-Requires accurate model of system -High online computational requirements -Complexity in design procedure -Hard and time consuming selection of constants and tuning of adaption gains
[18]	Adaptive PI controller	-Robust performance at different loading conditions	-Complexity in design procedure -Hard and time consuming selection of constants and tuning of adaption gains
[19]	MRAC&PI controller	-Low tracking error -Fast transient response -Robust performance at different	-Requires accurate model of system -Hard tuning of adaption gains
[20]	PI-PSO controller	-Robust performance against under uncertain grid impedance	-Precise selection of the predefined parameters -Necessitates expertise to obtain the desired response
[21]	PI-fuzzy controller	-Robust performance with irradiance variation -Don't require model of system	-Dependence of its implementation to the availably of training data -Hard selection of membership functions and fuzzy rules
	Proposed MRAC-PI controller	-Provides desirable dynamic response -Provides low grid current THD -Robust performance with irradiance variation -Robust performance with filter inductance variation -Guarantee system stability in the presence of uncertainty -Systematic procedure design -Fast convergence of the no initialized PI parameters	-Requires accurate model of system -Hard tuning of adaption gains

References

[1] Aourir M, Abouloifa A, Lachkar I, Aouadi C, Giri F et al. Nonlinear control and stability analysis of single stage grid-connected photovoltaic systems. International Journal of Electrical Power & Energy Systems 2020; 115: 105439. doi: 10.1016/j.ijepes.2019.105439

[2] Kabalcı E. Review on novel single-phase grid-connected solar inverters: circuits and control methods. Solar Energy

2020; 198: 247–274. doi: 10.1016/j.solener.2020.01.063

[3] Sampaio LP, da Rocha MV, da Silva SAO, de Freitas MHT. Comparative analysis of MPPT algorithms bio-inspired by grey wolves employing a feed-forward control loop in a three-phase grid-connected photovoltaic system. IET Renewable Power Generation 2019; 13 (8): 1379–1390. doi: 10.1049/iet-rpg.2018.5941

[4] Niazi K, Yang Y, Sera D. Review of mismatch mitigation techniques for PV modules. IET Renewable Power Generation 2019; 13 (12): 2035–2050. doi: 10.1049/iet-rpg.2019.0153

[5] Zeb K, Uddin W, Khan MA, Ali Z, Ali MU et al. A comprehensive review on inverter topologies and control strategies for grid connected photovoltaic system. Renewable and Sustainable Energy Reviews 2018; 94: 1120–1141. doi: 10.1016/j.rser.2018.06.053

[6] Zhu X, Chen K, Wang Y, Zheng H. Adaptive PID controller for cloud smart city system stability control based on chaotic neural network. Cluster Computing 2019; 22 (6): 13067-13075. doi: 10.1007/s10586-017-1197-5

[7] Pahari OP, Subudhi B. Integral sliding mode-improved adaptive MPPT control scheme for suppressing grid current harmonics for PV system. IET Renewable Power Generation 2018; 12 (16): 1904–1914. doi: 10.1049/iet-rpg.2018.5215

[8] Dang C, Tong X, Song W. Sliding-mode control in dq-frame for a three-phase grid-connected inverter with LCL-filter. Journal of the Franklin Institute 2020; 357 (15), 10159-10174. doi: 10.1016/j.jfranklin.2019.12.022

[9] Gao Y, Li X, Zhang W, Hou D, Zheng L. A sliding mode control strategy with repetitive sliding surface for shunt active power filter with an LCLCL filter. Energies 2020; 13 (7): 1740. doi: 10.3390/en13071740

[10] Yıldıran N, Tacer E. A new approach to H-Infinity control for grid-connected inverters in photovoltaic generation systems. Electric Power Components and Systems 2019; 1: 1–10. doi: 10.1080/15325008.2019.1689445

[11] Yang H, Zhang Y, Liang J, Liu J, Zhang N et al. Robust deadbeat predictive power control with a discrete time disturbance observer for PWM rectifiers under unbalanced grid conditions. IEEE Transactions on Power Electronics 2018; 34 (1): 287-300. doi: 10.1109/TPEL.2018.2816742

[12] Gholami-Khesht H, Monfared M, Taul MG, Davari P, Blaabjerg F. Direct adaptive current control of grid-connected voltage source converters based on the Lyapunov theorem. In: 2020 Ieee 9th International Power Electronics and Motion Control Conference (ipemc2020-ecce Asia); Tayland; 2020. pp.1-20.

[13] Shakeel FM, Malik OP. On-line self-tuning adaptive control of an inverter in a grid-tied micro-grid. Electric Power Systems Research 2020; 178: 106045. doi: 10.1016/j.epsr.2019.106045

[14] Raja BM, Houda R, Khadija D, Said NA. A discrete neuro sliding mode control with adaptive switching gain for uncertain nonlinear systems. In: 2018 15th International Multi-Conference on Systems, Signals & Devices (SSD); Hammamet, Tunisia; 2018. pp. 976–981. doi: 10.1109/SSD.2018.8570562

[15] Raja BM, Houda R, Khadija D, Said NA. A discrete adaptive second order neuro sliding mode control for uncertain nonlinear system. In: 2019 19th International Conference on Sciences and Techniques of Automatic Control and Computer Engineering (STA); Sousse, Tunisia, Tunisia; 2019. pp. 518–523. doi: 10.1109/STA.2019.8717283

[16] Tambara RV, Scherer LG, Gründling HA. A discrete-time MRAC-SM applied to grid connected converters with LCL-filter. In: 2018 IEEE 19th Workshop on Control and Modeling for Power Electronics (COMPEL); Padua, Italy; 2018. pp. 1–6. doi: 10.1109/COMPEL.2018.8460061

[17] Negi P, Pal Y, Leena G. Grid-connected photovoltaic system stability enhancement using Ant Lion optimized model reference adaptive control strategy. Differential Equations and Dynamical Systems 2020; 1: 1–23. doi: 10.1007/s12591-020-00525-9

[18] Elnady A, AlShabi M. Operation of parallel inverters in microgrid using new adaptive PI controllers based on least mean fourth technique. Mathematical Problems in Engineering 2019; 2019 (1). doi: 10.1155/2019/4854803

[19] Siddique AB, Munsi MS, Sarker SK, Das SK, Islam MR. Voltage and current control augmentation of islanded microgrid using multifunction model reference modified adaptive PID controller. International Journal of Electrical Power & Energy Systems 2019; 113: 492–501. doi: 10.1016/j.ijepes.2019.05.065

[20] Osório CR, Borin LC, Koch GG, Montagner VF. Optimization of robust PI controllers for grid-tied inverters. In: 2019 IEEE 15th Brazilian Power Electronics Conference and 5th IEEE Southern Power Electronics Conference (COBEP/SPEC); Santos, Brazil, Brazil; 2019. pp. 1–6. doi: 10.1109/COBEP/SPEC44138.2019.9065615

[21] Omar O, Ouassaid M. Power quality enhancement of grid-connected photovoltaic system using Fuzzy-PI control. In: 2018 International Symposium on Advanced Electrical and Communication Technologies (ISAECT); Rabat, Morocco, Morocco; 2018. pp. 1–6. doi: 10.1109/ISAECT.2018.8618807